NANOSYSTEMS: PHYSICS, CHEMISTRY, MATHEMATICS, 2014, 5 (4), P. 517–539

ELECTRONIC PROPERTIES OF MoS_2 MONOLAYER AND RELATED STRUCTURES

A. N. Enyashin[1], G. Seifert[2]

[1]Institute of Solid State Chemistry UB RAS, Ekaterinburg, Russia
[2]Physical Chemistry, Dresden University of Technology, Dresden, Germany
enyashin@ihim.uran.ru, gotthard.seifert@chemie.tu-dresden.d

PACS 61.46.-w, 61.50.Ah, 61.72.-y, 61.82.Fk

The present review provides an overview of the transition metal dichalcogenides discovered newly at the level of two dimensions. A special emphasis is given to the electronic structure of semiconducting representatives of this family, which can depend on many factors like thickness, environment, mechanical strain and structural imperfections of the layers. Both calculations and experimental data available to date on example of MoS_2 compound evidence that, semiconducting dichalcogenide layers could become successful counterparts of graphene and nanosilicon as the materials of flexible nanoelectronics. However, current technologies for the fabrication of single mono- and multilayers of transition metal dichalcogenides still do not offer a large-scale and cost-effective product with the tuned quality to reveal all abilities predicted for these nanostructures.

Keywords: Inorganic graphene, molybdenum sulfide, layered chalcogenides, monolayer.

Received: 16 June 2014
Revised: 30 June 2014

1. Introduction

Layered compounds were intensively studied in the 1970's and early 1980's (see e.g. Levy [1]). Among them, a large variety of the pure and mixed compounds from the group of layered d-metal chalcogenides (TMCN) attracted the largest attention in view of their possible applications. The stratiform structure of these compounds, their sufficient chemical endurance and impossibility of the formation of monolithic structures under a high load predetermine their excellent antifriction properties, which found a wide technological application in the automotive and aerospace industries [2]. The latter stimulated an extensive research of structural, electronic and optical, chemical and galvanomagnetic phenomena within the bulks of these compounds, which were already reviewed at that time [3–5].

Recent fabrication and preliminary characterization of single layers of some metallic and semiconducting d-metal chalcogenides have demonstrated their high potential as the materials for two-dimensional electronics [6]. The first nanoelectronic devices — field-effect transistors, logical circuits, and amplifiers — have already been manufactured in labs [7–9]. Transparent TMCN monolayers with a distinct band gap can possess a high enough mobility for charge carriers at room temperature, high thermal stability and ultra-low standby power dissipation, which make them also attractive materials for the optoelectronics and energy harvesting industry.

All this has already renewed interest in their research by means of new experimental and computational techniques, which were essentially evaluated over the last 30 – 40 years. This review collects the present data about modulation of electronic properties of single and a few layer d-metal chalcogenides and their related systems upon such factors as mechanical deformation, intrinsic defects and impurities, interface formation. Taking into account the huge variety of compounds, special emphasis was given to their most famous representative —

molybdenum disulfide MoS2 as a prominent and prospective semiconducting compound with well established low-cost production.

2. Electronic structure of ideal monolayers and their slabs

As for many other types of layered materials, the electronic properties of layered chalcogenides are at a first glance determined by the bonding behavior within the layer and only modified secondarily by the interactions between the layers. Pioneering studies of the electronic properties of semiconducting MX_2 chalcogenides (M = Mo, W; X = S, Se) with hexagonal 2H crystal structure (see Fig. 1) date back to the 1950's and 1960's (Lagrenaudie [10], Fivaz and Mooser [11]). Also, heterojunctions of such componds were previously described in the 1980's [12].

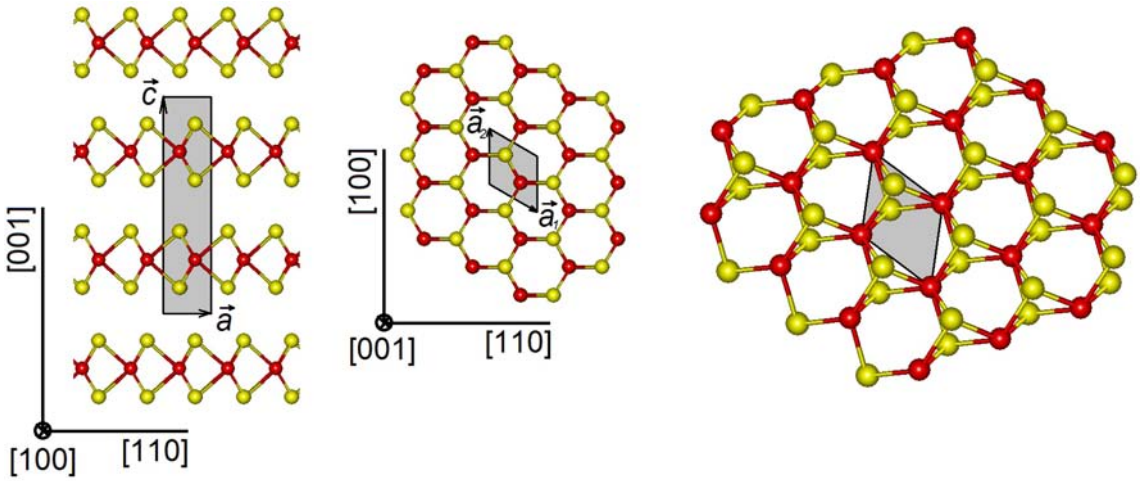

FIG. 1. Crystal structure of the bulk 2H-MoS_2 (space group $P6_3/mmc$) from the side and top views (along [100] and [001] directions) and a fragment of a single monolayer. Unit cells are shaded in gray

The structural units of TMCN layers and accordingly also of the corresponding bulk stacks can be deduced using group theory for d^4sp and d^5s electronic configurations of metal atom as having coordination number 6 and octahedral O_h or trigonal prismatic D_{3h} symmetry [13, 14]. While these coordination types have not been predicted for other electronic configurations (d^4s, d^3s^2, etc.), all layered dichalcogenides are composed either of MX_6 octahedra or prisms.

A first rough qualitative picture of the electronic structure of a single TMCN triple layer (X–M–X) structure can be deduced from a simple ligand field model. Formation of MX_2 compound is possible due to XsXp–MdMs hybridization and full occupation of the s- and p-shells of chalcogen atoms by 16 electrons. Towards that end, metals of IVb, Vb and VIb group keep 0, 1 or 2 d-electrons, respectively. In the case of the trigonal prismatic coordination of the metal, the d-states split into a1, e′ and e″ states, and from this picture, a simple band structure of a single layer TMCN can be understood (Fig. 2).

E.g., in the case of MoS_2, the lower part of the valence band is determined by the Mo-d–S–p 'bonding' states, followed by the almost 'non-bonding' d_z^2, d_{xy} and $d_{x^2-y^2}$ states at Mo. The band of the 'antibonding' Mo–d–S–p states are located above. Consideration of the 6 Mo valence electrons and a formal charge of -2 for the sulfur gives a formal charge of +4 for Mo in MoS_2. The 'd_z^2-band' is fully occupied, easily explaining the semiconducting behavior of MoS_2. The same qualitative picture holds for $MoSe_2$ and the sulfides and selenides

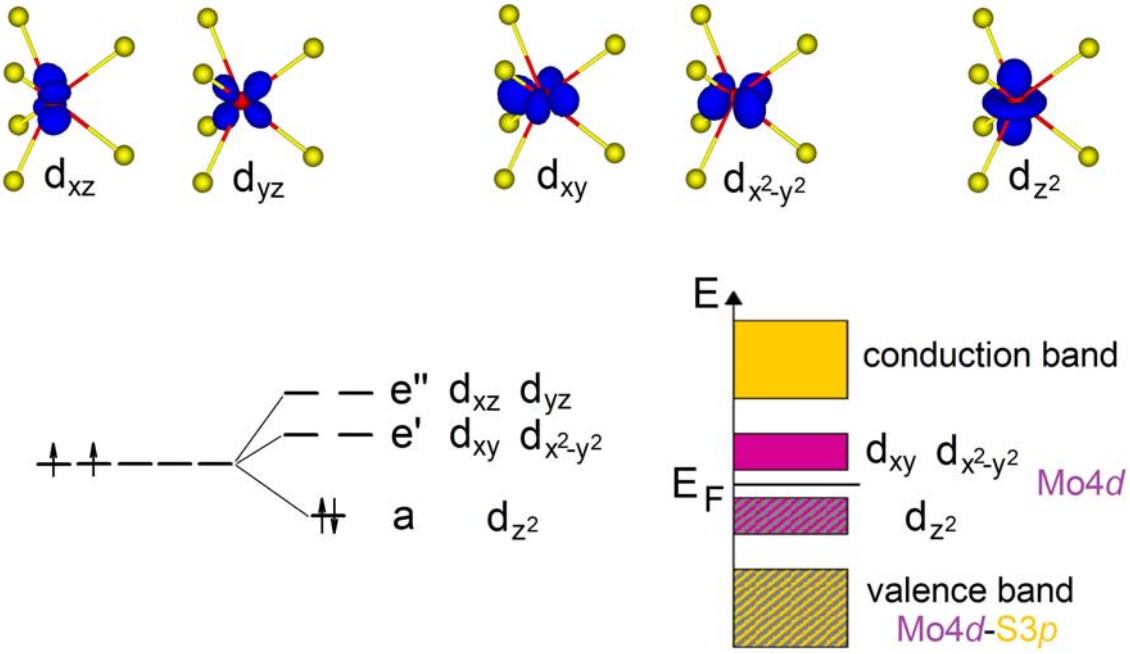

FIG. 2. Ligand field picture and corresponding d-orbitals for a trigonal prismatic coordination (D3h symmetry) in a d-metal dichalcogenide with a d2 configuration of metal atom and schematic band structure for a single MoS_2 layer

of Tungsten. I.e., the upper edge of the valence band and the lower edge of the conduction band are determined by metal d states. This model also explains why the chalcogenides of the group Vb metals (Nb, Ta) are metallic. Five valence electrons at the metal lead to a half occupation of the 'd_z^2-band'. The Sulfur states are predominantly involved in the M–S bonding, and therefore, in the stability of the structure, but play only a minor role in the electronic transport and optical properties. Since the sulfur atoms are 'saturated' and the metal d-states do not range out of the S–M–S triple layer, this simple model does not make a difference between the electronic structure of a single triple layer (1H structure) and the 2H-bulk structure. It also qualitatively explains the inertness and robustness of the TMCN surface. However, this model oversimplifies the real situation to some extent, as was already discussed by Mattheiss [15]. Mattheiss showed that a realistic size of the ligand field is not sufficient to produce a semiconducting gap, but consideration of the hybridization between the d_z^2, d_{xy} and $d_{x^2-y^2}$ states for Mo qualitatively gives the proper band splitting with a fully occupied narrow d-subband in the case of MoS_2 and half-filled for the group Vb TMCNs.

The first semi-empirical tight-binding calculations of the band structure for the bulk layered chalcogenide have already been performed, only in two-dimensional limit and assuming the similarity in the electronic properties of the bulk and single layer crystals [16]. Indeed, the comparison of the results [16] with APW calculations [15] confirmed this similarity of the 1H and the 2H band structure of MoS_2. Yet, late calculations by Galli et al. within a single DFT GGA scheme [17] have established a fine difference in the band structure of MoS_2 of different dimensionality: close to the Γ-point, due to the interlayer interaction, the splitting becomes larger, leading to transition from a direct gap (1H single layer) to an indirect gap (2H bulk allotrope) (Fig. 3).

The uppermost states at the Γ-point of the valence band originate mainly from d_z^2 orbitals on Mo atoms and contributions of p_z orbitals on S atoms. Due to the antibonding nature of these states, their energy diminishes with increasing interlayer distance and decreasing of the

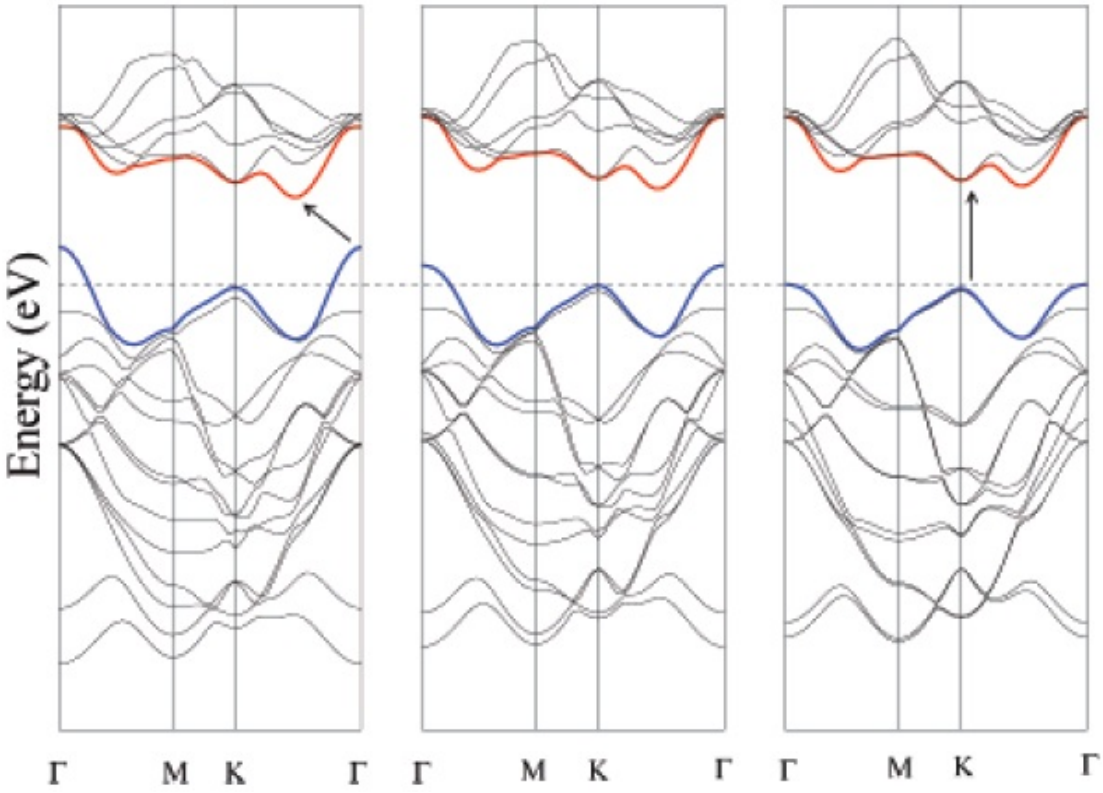

FIG. 3. Band structure of 2H-MoS_2 with increasing interlayer separation w (2.58 Å, 2.98 Å, and 3.58 Å — from left to right). For comparison, the energies are aligned with respect to the valence band top at the K-point. (Adapted from [17])

layer-layer interaction [17]. Conversely, the states at the top of the valence band and the bottom of the conduction band near the K-point, which are nearly exclusively d_{xy} and $d_{x^2-y^2}$ states for Mo, are accordingly unaffected by a change in the interlayer separation. Therefore, the gap between the valence band and the conduction band remains nearly constant at K ($\sim$ 1.8 eV GGA) with increasing interlayer separation, whereas the energy of the states at the top of the valence band at Γ decreases — see Fig. 3. For the limiting case of infinite layer separation (1H — single layer) the gap is determined by the states at the K-point and a transition from an indirect gap (Γ →K) to a direct gap (K→K) semiconductor. This behavior was confirmed by Lebegue et al [18].

The results were also confirmed experimentally [19,20]. Of course, the discussion of the variation of the band-structure on the basis of KS-LDA or KS-GGA orbital energies, especially with respect to size and character of the gap, has to be viewed with caution. However, quasi-particle calculations within the GW approximation qualitatively confirm this picture [21].

Kuc et al. [22] studied in more detail also other semiconducting and metallic TMCN with respect to the number of layers within multilayered slabs. The results of their DFT GGA calculations showed similar behavior to MoS_2. When going from the bulk 2H-structure to a single 1H-WS_2 layer, the system becomes a direct gap semiconductor with an increase of the gap from about 1.3 to 2.1 eV, respectively [16]. This phenomenon has already been observed by the authors when switching from a double-layered slab to a single layer. It is worth noting that the shape of the d-bands in the band structure of NbS_2 slabs also demonstrates the drift

of maximum and minimum at Γ and $1/2(\Gamma$–K) points by the variation of the number of layers, yet, these systems always remain metallic, due to the half-occupied d_z^2 band.

3. Electronic structure of the monolayers under mechanical deformation

Measurements of the stiffness and failure strength of MoS_2 monolayers and bilayers using atomic force microscopy [23] demonstrate the elastic mechanism of their deformation with an effective Young's modulus of 270 ± 100 GPa. Breaking occurs at an effective strain between 6 and 11 % with the average breaking strength of 23 GPa. These results show that single layers of chalcogenides possess exellent mechanical properties and could be suitable for a variety of applications such as reinforcing elements in organic composites and for fabrication of flexible electronic devices. Yet, all aforementioned theoretical studies of electronic structure of TMCN layers implied their ideal planar and strain-free structure. However, the semiconducting properties may be essentially changed under strain after embedment into real electronic devices, e.g. due to bending or stretching induced by the surface of a substrate or by a polymeric matrix. This problem has been considered in a few recent theoretical works.

The electronic properties of MoS_2 single and double layers under tensile or compressive biaxial strain have been investigated within the DFT GGA scheme [24]. The value of the band gap of mono- and bilayer systems reduces upon the application of any kind of deformation, which is in agreement with similar studies on the variation of the energy band gap as a function of pressure in the bulk MoS_2 [25]. For the monolayer, a transition from direct-to-indirect gap can be observed upon the application of relatively small strain ($\sim$ 2 %), when the energy of the top band of occupied states increases at Γ-point and energy of the bottom of unoccupied band decreases at K-point. A large tensile strain of about 8 % or a compressive strain of about 15 % should already lead to the semiconductor–metal transition. Application of uniaxial strain to single layered MoS_2 as well leads to a reduction of its band gap and transforms it to an indirect band gap semiconductor [26]. According to the more sophisticated quasiparticle GW calculations, for a strain of 1 %, the single MoS_2 should still have a direct gap, but for larger strains the transition to an indirect gap was confirmed [27].

The theoretical gap of MoS_2 monolayer reduces linearly with the stretching, until the material eventually becomes metallic at a certain strain level [24, 26]. This phenomenon can be interesting for possible application in nanoelectromechanics and optoelectronics engineering. Stretched semiconductors are likely to expose states near the Fermi level due to elongated bonds with a weaker orbital overlapping, which hence would not contribute essentially to electrical conductance. Thus, simple analysis of the band structure of strained semiconductor may not be sufficient and the transport properties should be elucidated.

First quantum conductance calculations on the mechanically deformed monolayers of MoS_2 and WS_2 were performed using the nonequlibrium Green's functions method combined with the Landauer-Büttiker approach for ballistic transport together with the density-functional-based tight binding method DFTB [28]. While DFTB calculations of the band gap response on the applied biaxial isotropic strain were found to be in agreement with *ab initio* data [24, 26], they also revealed a significant increase in the electrical conductivity at the Fermi level (Fig. 4). At the critical strain level ($\sim$ 11 %), when the band gaps of semiconducting layers vanish to zero, the transport channels are completely open and current flow is enabled. The electronic transport in the case of isotropic deformation (tensile or compression) does not depend on the direction of the current and remains almost the same for both *zigzag* and *armchair* directions of the layer.

The electron conductivity of MoS_2 monolayer under uniaxial strain demonstrates a different behavior [28] being applied in the parallel or in the perpendicular directions to the

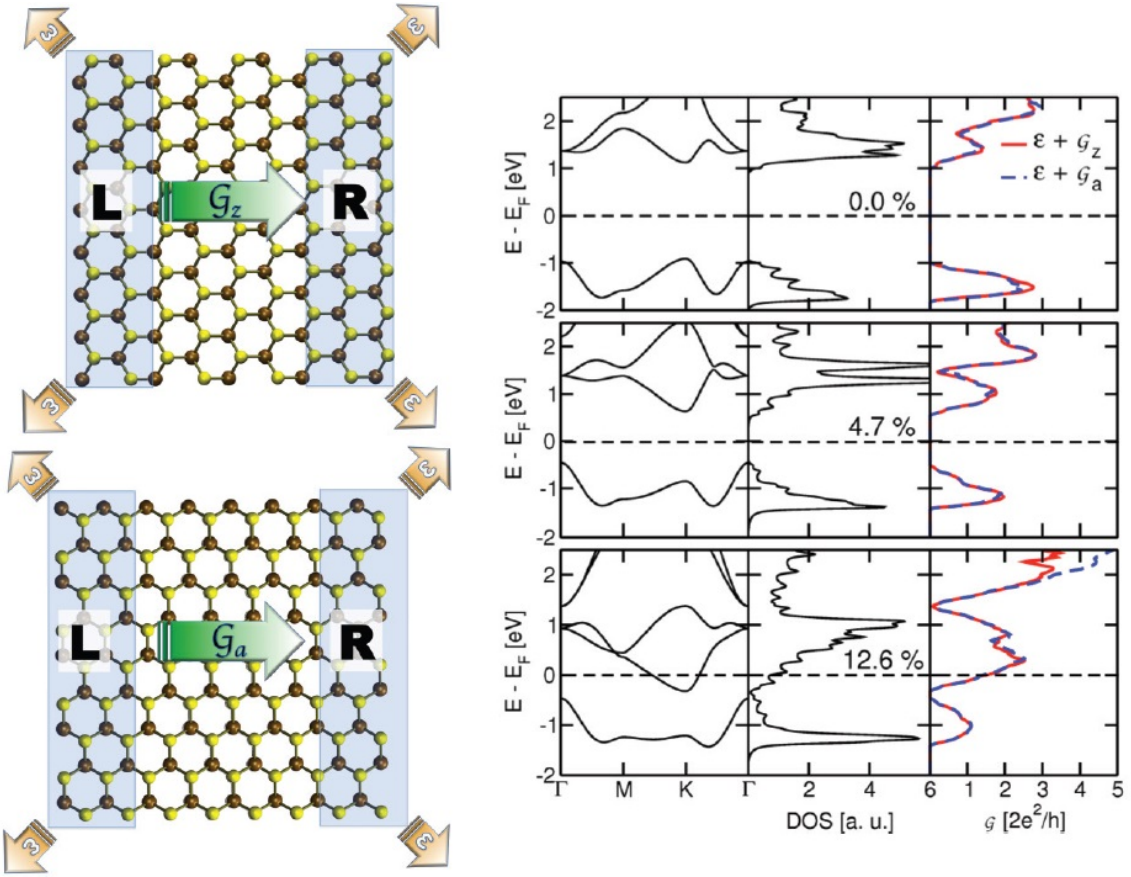

FIG. 4. Band structure, density of states and electron conductivity of MoS_2 monolayer under isotropic tensile strain as revealed by nonequlibrium Green's functions method in DFTB approach. Ga and Gz denote electron conductivity along armchair and zigzag directions of the layer, respectively. Adapted from [28]

transport axis. Even under high strain, the monolayer still shows semiconducting behavior with the known tendency of the band gap reduction. Yet, the electron conductivity of such strained monolayer would be predetermined by the direction of strain relative to the direction of current. Strain perpendicular to the current reduces the band gap without a significant change in the conductivity. In contrast, strain in the same direction as the current results in a reduced band gap, and also in reduced conductance for electron energies lower than the Fermi energy level. At energies higher than the Fermi level, such strain enhances the conductance drastically. Similar calculations performed on example of metallic NbS_2 monolayer have shown that the magnitude of conductivity may be also varied upon both isotropic and uniaxial deformations. These results highlight the importance of the strain direction for nanoelectromechanical applications of semiconducting as well as metallic layers. Noticeably, the critical strain for semiconductor-metal transition is too close to the limit of mechanical stability of this material under stretching, which is experimentally characterized by failure strain 6 – 11 % [20].

Besides 'in-layer' deformations, a certain interest should be devoted to the influence of the bending of TMCN layers on their electronic properties. The first clues on the band gap behavior and type of transition by this deformation mode have been obtained by numerous experimental and theoretical studies of chalcogenide nanotubes — in fact, the layers bent into nonsuture cylinders [29–33]. The band gaps of all semiconducting sulfide nanotubes are defined by the degree of curvature, and are smaller than the band gap of their planar counterparts.

Moreover, the type of the transition within nanotubes can be different and is defined by the folding of band structure of two-dimensional system along certain direction. E.g., the gap size of *zigzag* MoS_2 nanotubes is intimately related to that at the K-point in MoS_2 monolayer [29]. It gives evidence that bending of an infinite monolayer should lead to the reduction of the band gap and possibly to a change in the transition type, depending on the direction of the bending.

The locally bent parts can occur within a monolayer even without any external action, but due to thermal excitation. HRTEM, AFM and optical measurements reveal spontaneous rippling of MoS_2 layers [34]. The intrinsic dynamics of MoS_2 monolayer with the formation of oscillating ripples and its influence on the electronic structure and the conductance was studied by means of DFTB method in conjuction with Born-Oppenheimer molecular dynamics [35]. Both experimental and theoretical studies estimated the average characteristic length of ripples as 6 – 10 Å at a typical layer length of 60 – 100 Å. MD simulations unambiguously point on the thermal origin of this rippling. The average size of the ripples increases with temperature and the estimated ripple oscillation frequencies also increase. Expectedly, the phenomenon of ripple formation leads to a reduction in the band gap of MoS_2 monolayer due to the lowering of the lowest conduction band energies. Although, the transport calculations using DFTB method reveal a drastic reduction of the conductance in the direction across a ripple: in the most distorted structures, the transmission decreases 75 % compared to that of the flat layer.

It is noteworthy that experimental [34] and theoretical [35] studies of rippling formation have been performed on an example of the membranes — free parts of MoS_2 monolayer, which were not in contact with the substrate. The effect of the substrate on the mechanical deformation of a deposited TMCN layer has not been systematically studied yet. Though, it can be speculated that it may be depend on the strength of interfacial bonding. In the case of weak van der Waals interaction, the rippling can be suppressed, and the layer flattening would lead to the conductivity of ideal flat layer. The influence of a strong interface interaction is less predictable. It may lead not only to the flattening, but also to the stretching or tensile deformation of layer, which can reduce its conductivity, as was discussed above.

On the other hand, simulation of nanoindentation experiments, using an atomic force microscope, of single MoS_2 layers suspended over circular holes [20], shows the exceptional electronic robustness of the MoS_2 sheets towards local mechanical deformation [35].

4. Intrinsic conductivity of defect-free monolayers

The structure of layered chalcogenide semiconductors results in a highly inert surface with a relatively low defect concentration, which enables the fabrication of field effect transisors (FETs) with an intrinsically low field-effect threshold. The semiconductor gap makes the realization of FETs based on these materials even more attractive than those of graphene, where the missing gap creates serious problems for its application in corresponding devices. Field effect transistors of WSe_2 with a high mobility of charge carriers were fabricated [36]. However, these WSe_2 based transistors were characterized by high doping levels and showed reasonable *trans*-conductance characteristics only at low temperatures. Consequently, the fabrication of FETs based on single and a few layered MoS_2 has been demonstrated, but the observed electron mobility in the single layer MoS_2 is unexpectedly low (from 0.1 – 10 to tens of cm^2 /(Vs)) [6, 8,37]. These materials were also characterized as doped semiconductors, and their low mobility of charge carriers was explained by high density of charge trap states within the MoS_2 layer. Concurrently, the use of hafnium oxide as gate dielectric allows one to reach mobility in single-layer MoS_2, at least to 200 cm^2/(Vs) at a room-temperature, similar to that of graphene nanoribbons [7].

Indeed, already the first electrical measurements have clarified that the conductivity of bulk chalcogenides can be widely varied, depending on the purity of samples (see reviews [1,4]). A typical dependence for logarithm of resistance on inverse temperature for bulk layered chalcogendies consists of two regions with activation energies < 0.1 eV at low temperature and 0.4 – 0.9 eV at high temperatures ($\sim$ 400 K and above), which can be attributed to extrinsic and intrinsic conductivity, respectively. The problem of purification of these compounds and uncontrollable distribution of an impurity may explain the poor reproducibility of the measurements, even for samples with formally equal doping levels. The electrical conductivity measured for the crystals of dichalcogenides grown in various conditions may vary more than 106 times for MoS_2, 105 for $MoSe_2$ and 103 for WSe_2 [38]. The reason for these deviations was explained not only by the doping content, but also by the temperature controlled size of the chalcogenide grains. An annealing of the samples can lead to the increase of average size of the grains, i.e. to decrease the number of intergrain contacts with a high electrical resistance.

The understanding and revelation of intrinsic conductivity is important to determine the maximal possible performance and the feasibility of a chalcogenide layer as a material for nanoelectronics. Already, Fivaz and Mooser [11] have shown that the mobility in bulk metal chalcogenides, such as MoS_2, is limited by the phonon scattering — interaction with optical phonon modes ($A2''$ — mode 481 $cm^{-1} = 0.06$ eV, the IR-active antisymm vibration perpendicular to the MoS_2 plane). This has been confirmed and discussed in detail for the single MoS_2 layer by Kaasbjerg et al. [39]. They have calculated effective electron mass, the scattering rate and phonon-limited mobility in the layer as a function of carrier energy, temperature and carrier density. The intrinsic electron mobility was characterized as dominated by optical phonon scattering and estimated as ~ 410 $cm^2/(Vs)$. These findings suggest that low experimental mobilities, on the order of ~ 1 $cm^2/(Vs)$ reported in Ref. [6, 8], are indeed dominated by other scattering mechanisms, e.g., by scattering on some charged impurities or defects. Obviously, the latter is screened using deposition of a high-k dielectric material on MoS_2 surface. A comparison of the temperature dependence of the mobility in samples with and without the top-gate structure performed in [39] clarifies in this manner the observed enhancement in the mobility to ~ 200 $cm^2/(Vs)$ [7].

5. Possible routes for fabrication of monolayers and the origin of defects

There are several possible origins for scattering centers in the layers of TMCN, which are able to affect electronic properties: vacanices within metal or chalcogen sublattices, point-like reconstructions and extended line defects, grain boundaries, doping or adsorbed atoms. To a large extent, the types and amounts of these centers and their combinations are defined by the history of the sample. At present, a few top-down and bottom-up fabrication techniques have been evaluated.

The first of them implies an exfoliation of a bulk layered crystal. For example, the most inspiring measurements of the mobility and FET design have been performed on samples of MoS_2 layers extracted from a naturally occurring form of MoS_2 — molybdenite mineral — using a micromechanical cleavage technique [6, 7]. The strength of strongest MoS_2 monolayer membranes created from molybdenite is about 11 % of its Young's modulus, which is quite close to the upper theoretical limit calculated in the approximation of ideal lattice and indicates that such material can be highly crystalline and almost defect-free [23]. However, the gate-controlled character of the conductivity suggests the presence of at least charged defects. These can be likely presented in molybdenite by substitutionally doping Re atoms in amount from a few ppm to 1 % [40]. Currently, there is no route known for the purification of molybdenite, and the minor admixtures cannot be removed from such prepared layers. Definitely,

cleavage could be processed from the synthetic chalcogenide bulk crystals, grown using gas transport techniques [38]. Yet, this option is not explored profoundly and this technique is not sufficiently evaluated for this purpose. Layers of synthetic chalcogenide crystals are known to contain dislocations, grain boundaries, intercalated metal atoms, which would require an additional annealing. Another noteworthy disadvantage of micromechanical cleavage is low mass production. The desired single layer particles are barely present in the wide distribution of the cleaved multilayered flakes.

An early known mass production method employs chemical exfoliation and includes preliminary intercalation of the bulk chalcogenide by lithium or other alkali metal and subsequent sinkage of intercalate in aqueous solvent [41]. Apparently, it is limited by the chemical stability of chalcogenide lattice against such reducing agents and the final products will contain numerous defects such as vacancies or even amorphous nonstoichiometric phases. To overcome the problem of an intercalant, the utilization of direct liquid exfoliation of the bulk compound can be suggested, which would depend on the solubility of the compound in an appropriate solvent. Recently, it was demonstrated that many layered chalcogenides can be efficiently and in large quantities dispersed in a range of common solvents [42]. Due to the physisorptive nature of exfoliation, the quality of the final product in this case would be as well predetermined mainly by the state of the bulk crystal itself. Despite of the advantages of the latter technique over mechanical cleavage and chemical exfoliation, it also gives a mixture of mono- and few-layer flakes containing trace amounts of solvent .

The extrusion of the single layers from the 'mess' of multilayers is a common feature of top-down methods, which hampers the subsequent transfer of the layer onto a substrate and further operations. The bottom-up approach may be a more successful alternative, providing controllable deposition of the material with required number of the layers on desired substrate. By this means, much progress has been achieved in the fabrication of single-layered MoS_2 islands with the sizes varying from dozens atoms [43] to dozens nanometers [44] by subsequent S and Mo atomic depositions and annealing on a metal surface. The large-area growth of MoS_2 thin films with scalable thickness and size up to several millimeters was achieved using chemical vapor deposition (CVD) method on SiO_2/Si substrates with different pretreatments [45, 46] or using thermolysis of thiomolybdates on SiO_2/Si or sapphire [47]. It is noteworthy that the bottom-gated transistors, constructed from such deposited MoS_2 monolayers, have frequently demonstrated lower carrier mobility, than those built from mechanically cleaved monolayers. This is clear evidence that the MoS_2 layers prepared under such extreme conditions can have randomly grained structure and contain numerous defects, including vacancies and dislocations [46].

Thus, the challenging application of single-layered chalcogenides in electronics also keenly urges on the search for appropriate synthetic routes, which could provide the high purity and crystallinity of the layers together with the ease, accuracy and low cost of manipulation on a layer after its production. While these methods are still being evaluated, essential progress has been achieved in the defect characterization of TMCN monolayers at an atomistic level.

6. Intrinsic defects within the monolayers and their influence on electronic structure

One of the most simple and prevalent intrinsic defects, which can occur within the lattice of chalcogenide layers, are single atom vacancies. The most profound study on the formation of these defect types by irradiation treatment was performed by Komsa et al. [48]. DFT-GGA calculations for a large family of TMCNs layers have been employed for the estimation of vacancy formation energies, threshold energies for atomic displacements and displacement cross sections under electron irradiation. Sulfur vacancy within a semiconducting layer leads to the

occurence of an occupied bonding type vacancy state close to valence band gap maximum and an empty antibonding state in the mid gap, which stabilizes structure. The formation energy for the vacancy in a non-metal sublattice was found to be smaller than the displacement threshold energy in the same compound. The calculated data allowed to estimate the electron threshold energies. The formation energies for selenides and tellurides are smaller than for sulfides, but due to the higher atomic weights, the creation of vacancies through ballistic electron impacts requires significantly higher electron energies. In the case of MoS_2, $MoSe_2$ and $MoTe_2$ electron threshold energies were estimated at about 90, 190 and 270 keV, respectively. Thus, particularly, the production of S vacancies is within the energies commonly used in TEM studies. The displacement thresholds for chalcogen atoms in the top plane facing the beam proved to be considerably higher than for the bottom chalcogen layer as the displaced atom is 'stopped' by the other layers. The threshold energies for the metal vacancies are also higher, due to higher coordination number; e.g., the electron energy to displace Mo atom in MoS_2 was estimated as 560 keV, which is far beyond the stability of the monolayer. Yet, the formation of such defects with a slight chalcogen surplus in the samples cannot be excluded during the synthesis of chalcogenide layers. These theoretical results were supported by an experimental TEM study of natural molybdenite MoS_2 layer evolution under 80 keV electron beam. During continuous imaging, an increasing number of vacancy sites (exclusively on the S sublattice) were found (Fig. 5). The contrast TEM images even allowed us to distinguish single and double vacancies.

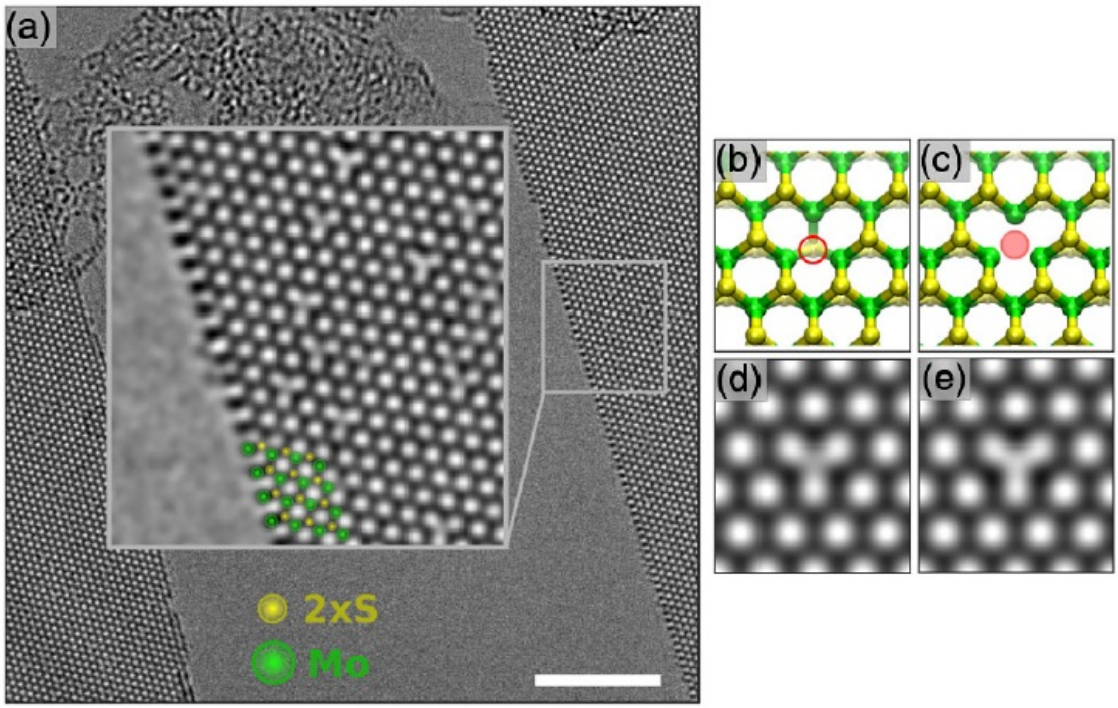

FIG. 5. AC-HRTEM image of a single MoS_2 layer under electron irradiation shows an increasing number of point defects: S single and double vacancies (scale bar is 5 nm) (a). Structure models and corresponding simulated HRTEM images for both vacancy types are shown in (b),(d) for the single (b,d) and for the double vacancy (c,e). Adapted from [48]

The possibility of vacancy formation in the layers under electron irradiation may not only be an objectionable effect, but could also be used for the modification of the electronic structure using single atom doping. The authors [48] have suggested that the created vacancies

can be subsequently filled with different species (other than chalcogen), deliberately injected into the TEM chamber. The formation energy of substitutional defects in MoS_2 by isoelectronic O, S, Se, Te, electron donating F, Cl, Br, I and accepting N, P, As, C, Si atoms have been found as energetically favored. The filling of S vacancies by the atoms was detected experimentally in TEM images, yet, their nature was not identified. Furthermore, HRTEM experiments have been established for the production, diffusion and agglomeration of sulfur vacancies within MoS_2 layer under electron irradiation [49]. Single vacancies can be mobile under an electron beam and tend to agglomerate into lines of a few different kinds, which orientation should be sensitive to mechanical strain.

Atomic-resolution annular dark field (ADF) imaging on abberation-corrected scanning transmission electron microscope (STEM) was performed on MoS_2 samples, which were CVD grown on SiO_2 substrate and posses n-type conductivity [50]. As was mentioned above, synthetic chalcogenide crystals can possess a large number of dislocations. Indeed, a rich variety of intrinsic structural defects such as point defects and dislocation cores, grain boundaries were directly observed within single MoS_2 monolayers. Grain boundary structures in TMCN binary compounds were identified to be more complex than those in graphene and consisting of 4|4, 5|7, 6|8 and 4|6 dislocation core structures containing homonuclear Mo-Mo bonds or hyperco-ordinated S atoms (Fig. 6). A rich variety of the defects and their complex structures give rise to a wealth of possible honeycomb orientations of neighboring grains. The electronic structures of the experimentally observed grain boundaries were explored using DFT calculations. In all cases, the presence of a grain boundary causes the occurrence of new states in the band gap of MoS_2. Fig. 6c shows the band structure and local density of states for so-called 4|4E grain boundary as an example. It can be imagined as a perfect 1D metallic quantum wire embedded into the semiconducting MoS_2 matrix with dispersive bands crossing the Fermi level, which was proven by visualization of partial charge density.

The crystal structure of CVD-grown MoS_2 microcrystals on Si/SiO_2 substrate was also analyzed using TEM, ADF-STEM and electron diffraction techniques by van der Zande et al. [51]. A few types of microcrystals were identified: single-crystal triangles with Mo or S edge terminations and polycrystalline crystals. The first type of nanoparticles has been characterized by a negligible amount of point defects, which however were readily formed under extended imaging. The polycrystalline nanoparticles were described as merged by means of line defects represented as with tilt or mirror twin boundaries formed by 8- and 4-memebered rings in such manner, that hexagons of honey-comb structures of two neighbor grains are oriented under 180 ° angle. DFT calculations performed on a set of a few defective structures have also given evidence for the appearance of mid-gap states, which are mainly localized at the boundary atoms.

Other types of grain boundaries were identified in double layers of MoS_2 using HRTEM imaging combined with DFTB calculations [52]. The grain boundaries can be represented as a line defect consisting of either homonuclear Mo–Mo bonds or of two S bridge atoms (Fig. 7), which would link always two grains with *zigzag* either S or Mo termination. The high stability of these types of covalent linking was demonstrated by MD simulations, even at 600 K. Calculated DOS for all defects includes localized trap states near the Fermi level and in the band gap region. The electronic properties of layers containing such defects should stem mainly from the edge states of the two opposite domains, in a similar way as described in the literature for triangular MoS_2 nanoplatelets and nanostripes with metallic-like edges [53, 54].

The results of DFT calculations [50–52] unambiguously claim the presence of mid-gap states in semiconducting TMCN layers with grain boundaries independent of their origin. These states could affect the electrical transport and optical properties of a semiconductor. Van der

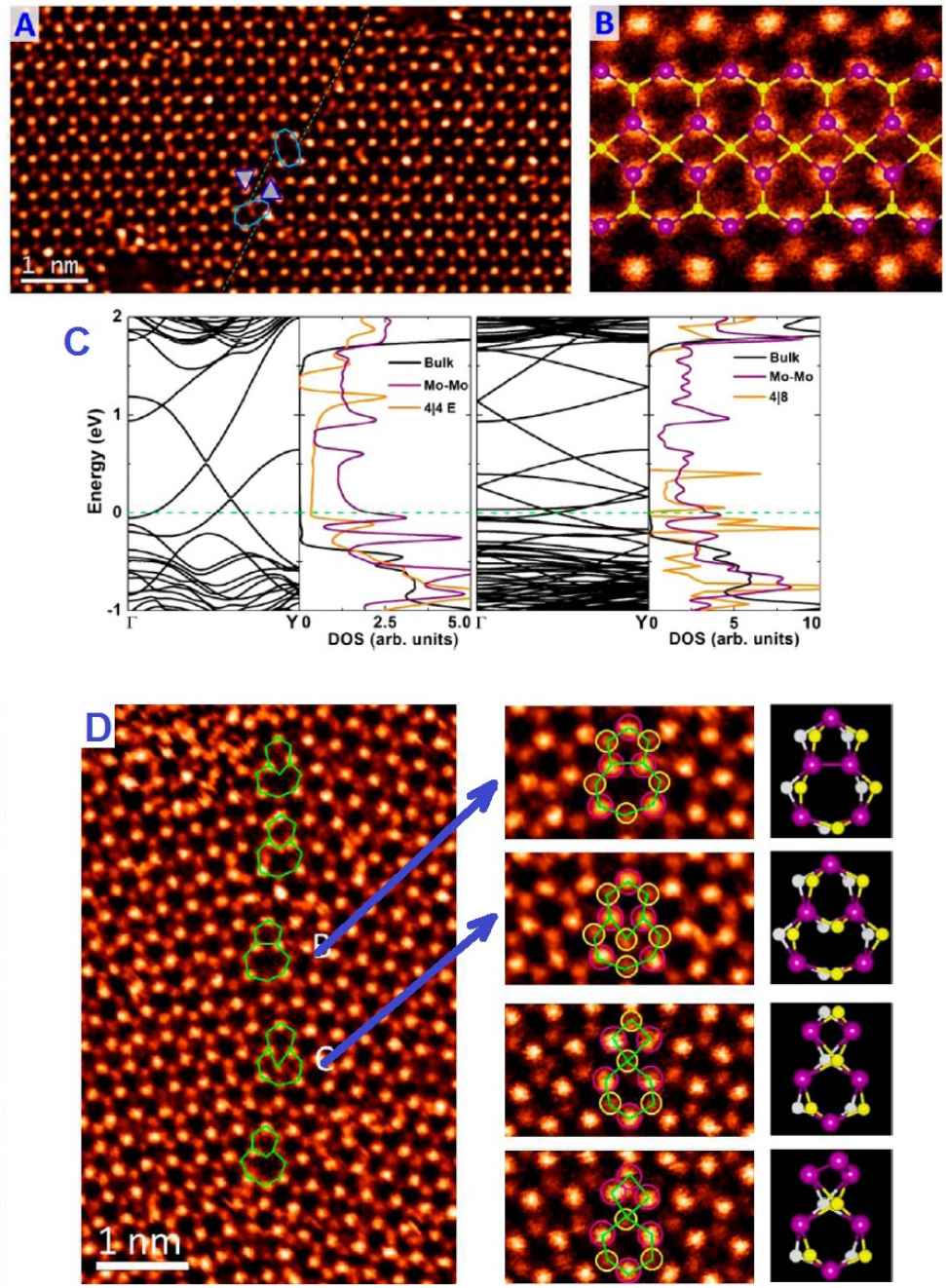

FIG. 6. STEM-ADF images and structural models of some grain boundaries in single layer MoS_2: (A) a 4–4P 60 ° grain boundary; (B) magnified part of (A) with the structural model overlaid; (C) Band structures, total and partial densities of states of the 4–4E and 4–8 grain boundaries; (D) Small-angle grain boundaries consisting of 5–7, 6–8 and 4–6 fragments in single layer MoS_2 and their 3D structural models. Adapted from [50]

Zande et al. have engineered a set of FET devices from MoS_2 islands containing a single grain boundary and studied the conductance across and along both twin and tilt type grain boundaries [51]. The pristine devices constructed on a single MoS_2 grain show n-type behavior with mobilities of 3 – 4 $cm^2/(Vs)$, which is comparable to those reported for gated FETs

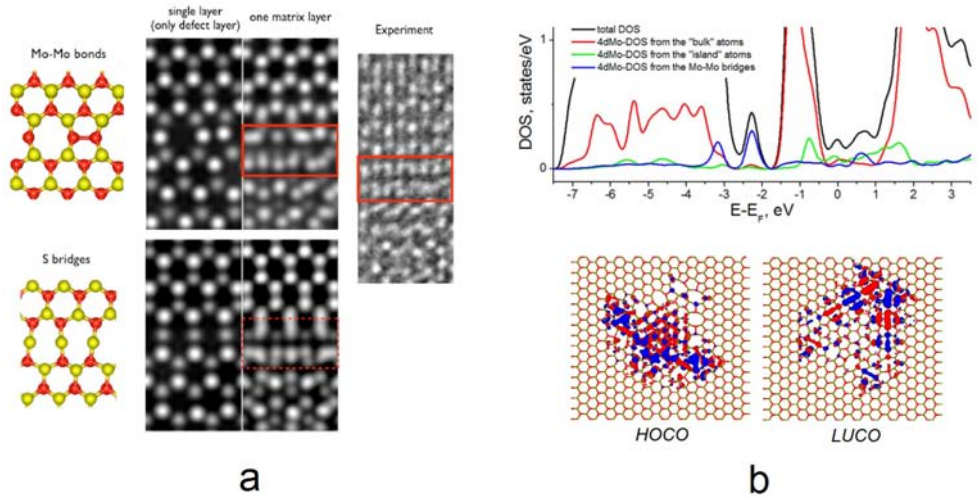

FIG. 7. (a) Structural models, calculated and experimental HRTEM images of homonuclear line defects in single and double layer MoS_2. The central part shows the images simulated for the Mo–Mo bond defect and the –S– bridges defect. The experimental data show a consistent match with the simulated images for the defect with Mo–Mo bond. (b) Total and partial DOS calculated for the single MoS_2 layer with the embedded island interlinked either via three Mo–Mo line defects bonds. Γ-point isosurfaces of highest occupied and lowest unoccupied crystal orbitals (HOCO and LUCO) are also depicted. Adapted from [52]

fabricated from mechanically exfoliated MoS_2 in the absence of high-k dielectrics [6, 8]. The transport across a twin grain boundary shows nearly identical performance to pristine devices, indicating a minor effect on channel conductivity. The electrical characteristics of the devices measured along the boundaries are different and demonstrate a 25 % larger on-state conductivity and 60 % larger off-state conductivity compared to the pristine material. Furthermore, the measurements indicate that these few-atom wide twin boundaries have similar conductivity of up to 1 μm wide strip of pristine material. In contrast to the mirror twin, FET devices of tilt boundaries show a decrease in conductance in both parallel and perpendicular directions with decreases of 5 – 80 % compared to pristine devices. Such variability points to a tight influence of the boundary structure on electric properties.

Electron transport measurements have been performed also by Najmaei et al. [55] on the samples of defective single and a few layered MoS_2 sheets with a larger variation of grain boundary types described in Ref. [50]. The results for generic electrical performance of these devices are quite similar to the aforementioned results: n-type semiconductivity with an average mobility of 4 cm^2/(Vs) was observed, independent of the sheet thickness.

Thus, the structure of the grain boundaries and mutual orientations of grain honeycombs visualized in Ref. [50–52] reveal that this type of intrinsic defect often would not be removed even after annealing or additional healing by chalcogen or metal atoms. Of course, this fact could be used for the engineering of electronic properties of a semiconducting layer. Yet, control of defect formation or grain boundary growth cannot be achieved. At present, the occurrence of intrinsic defects in an uncontrolled manner should be considered mainly as an interfering factor for the application of semiconducting TMCNs in FET devices. The charge carrier mobility can be poor reproducible from the device to device, depending on the uncontrollable content and orientation of boundaries, i.e. on the fabrication route. Low mobility, due to a scattering on the structural defects, obviously, cannot be easily increased using the appropriate electrostatic

environment. Thus, a careful growth technique should be always evaluated for TMCN semiconductors to provide a monocrystalline structure without grain boundaries and other intrinsic defects, which affect electrical performance.

Apart from intrinsic defects, the electron transport measurements of defective MoS_2 structures can be interfered with many other factors, like doping, substrate induced potential or resistance at the contacts of experimental setup. The theoretical calculations allow one to distinguish the role of these factors. In general, they confirm the peculiarities of intrinsic defects in transport properties. As well, they point to new phenomena, which still have to be proven in experiments. E.g., it has been theoretically predicted that a finite atomic line of S vacancies created on a planar MoS_2 substrate, like those designed in Ref. [49], can function as a pseudoballistic wire for electron transport [56]. Removal of surface S atoms introduces electronic states within the band gap. Each S vacancy introduces a symmetric molecular orbital of mainly Mod_z^2 character near the top of the valence band and a degenerate pair of molecular orbitals of mainly Mod_{xz} and d_{yz} character near the center of the band gap. Mixing of the degenerate orbitals on neighboring vacancies causes the gradual formation of two overlapping energy bands near the Fermi level, which create pseudoballistic electron transport channels.

The electronic properties and the quantum transport in MoS_2 monolayer containing one of several structural defects were studied by means of DFTB method in conjunction with the Green's function approach [57]. A rich set of point and line defects was taken into account: vacancies in Mo and S sublattices, holes, add-atoms, 4|8 and 5|7 Stone-Wales-like rearrangements as the fragments of grain boundaries observed in Ref. [50], the line defects and their loops as obtained in Ref. [52]. All types of defects studied in this work show significant changes in the electronic structure close to the Fermi level and introduce mid-gap states within the band gap of MoS_2 (1.5 eV in this approach). This has already been reported in previous studies on defective MoS_2 [48, 50–52]. The mid-gap states are strongly localized in the vicinity of the defects and are mostly of Mo4d type (Fig. 7b). Due to this localization, these defect states should be considered as scattering centers. Although the defect states reduce the band gap significantly, their scattering character prevents opening any new conduction channels close to the Fermi level. The occurrence of defects reduces the conductivity in comparison with the pristine layer at 1.2 eV above and below the Fermi level. Expectedly, the conductivity depends strongly on the type and concentration of the point defects. Surprisingly, the electron conductivity of the systems with point defects also becomes strongly dependent on the direction of current, namely, the conductivity is suppressed much stronger for the armchair transport direction. The only exception is the single S-vacancy, where the transport seems to be independent of the considered direction; e.g., in the case of transport in *armchair* and *zigzag* directions, the electron conductance of MoS_2 with a single Mo-vacancy (in amount 1 %), is suppressed by 75 % and 90 % compared with the pristine layer. Conversely, the single S vacancy (in amount 0.55 %) shows higher electron conductivity due to the electron injection directly to the conduction band. Furthermore, for Stone-Wales defects, the conductance is reduced by less than 50 % with respect to the pristine structure. The conductance perpendicular to the line defects also reduces with increasing channel length, keeping the band gap unchanged.

7. Impurities within the monolayers and their influence on electronic structure

As was shown for the example of a MoS_2 semiconductor, CVD grown layers often are not free of intrinsic structural defects and, obviously, the layers exfoliated from natural samples demonstrate a better structural quality. Despite this, natural samples can be heavily contaminated by other d-metals, usually by Re [40]. The latter may affect the semiconducting properties due

to formation of donor or acceptor levels as well as the electron mobility [6, 8] due to scattering or trapping on the charged point defects — the atoms of such a dopant.

The electronic structure of semiconducting MoS_2 layers, doped by substitution with Re atoms, was considered theoretically using DFTB method depending on the amount and distribution of atoms of dopant [58–60]. The single rhenium atoms in low concentration at Mo sites only slightly changed the DOS profile. This change manifested itself through the occurrence of an impurity level at $\sim$ 0.2 eV below the conduction band of MoS_2 and with a significant $5d$Re character (Fig. 8). These findings are reminiscent of an n-type doping of a semiconductor. A doping of MoS_2 monolayer by many separated rhenium atoms up to 1.6 % Re with random distribution does not change cardinally the DOS profile and leads to the increased intensity and the position of the band of the donor levels. The absence of large broadening at such high doping levels gives evidence that the electrons in the donor band should be strongly localized, which can be demonstrated using a visualization of the crystal orbitals for corresponding donor levels (Fig. 8). Clear localization of impurity states is also preserved for the case of island-like Re atom distribution. Though, with this type of distribution, the DOS profile of the impurity band is split into two bands, occupied and unoccupied. These bands are located at $\sim$ 0.5 eV and $\sim$ 0.1 eV below the conduction band of MoS_2, respectively. Gradual increase of the rhenium content leads to the occurrence of new impurity bands in the band gap of MoS_2 and to the increase of DOS of Re$5d$ states. The impurity states are also located exclusively in the band gap of MoS_2.

Apparently, a more drastic change of the electronic structure of a layered TMCN compound can be obtained due to the phase transition induced by doping. In addition to the allotrope formed from prismatic MX_6 units (1H structure), TMCN layers can be formed by the units with octahedral coordination (1T structure) [1]. In terms of crystal field theory, the splitting of d-orbitals in an O_h-MX_6 unit can be described as splitting into two groups: three degenerate $d_{xy,yz,xz}$ orbitals with low energy and two degenerate d_z^2 and $d_{x^2-y^2}$ with high energies (Fig. 9). For MoS_2 compound, in this case, the lowest d-orbitals are populated only with two electrons. The incomplete occupation of Mo4$d_{xy,yz,xz}$ orbitals in 1T-MoS_2 leads to the metallic ground state and also decreases the stability of this allotrope. Therefore, by doping the 1T-MoS_2 layers with an electron donating atom, the additional electrons occupy the Mo4$d_{xy,yz,xz}$ orbitals and increase the stability of the T-phase. On the contrary, when such doping occurs in the semiconducting 1H-MoS_2 allotrope, the electrons which are donated to the Mo4$d_{xy,yz,xz}$ orbitals and to the Mo4$d_{x^2-y^2}$ orbitals result in the metallic-like character of the electronic structure, and this causes destabilization of the lattice. Thus, the transition from the semiconducting 1H- to the metallic 1T-phase in MoS_2 may occur after adsorption of the electron-donating atoms of alkali metals or as a result of substitutional doping by atoms of d-elements, which can serve as electron donors (as Re, Tc, and Mn). DFTB calculations for both allotropes of MoS_2 monolayers and bilayers doped with different amounts of Re atoms support this tendency [60]. The higher the Re content is within $Mo_{1-x}Re_xS_2$ phase, the more stable 1T-$Mo_{1-x}Re_xS_2$ becomes. Recently, this phenomenon was proven by TEM study of related systems — multiwalled WS_2 nanotubes doped by Re, where both allotropes coexist. Yet, the same can be expected for the monolayers or thin flakes of MoS_2 and WS_2. Exceptional doping can induce new phase state and change the type of conductivity or at least facilitate a partial structural reorganization, which would lead to the change of mobility.

Substitutional doping of MoS_2 monolayer at the Mo site with single atoms of $4d$ elements and Re was considered in details by means of DFT LSDA calculations [61]. These results also demonstrated the n-type character of Re doping. To that end, the magnetic state of Re impurity with magnetic moment 1 μB was found lower in energy. In general, for all the substitutional

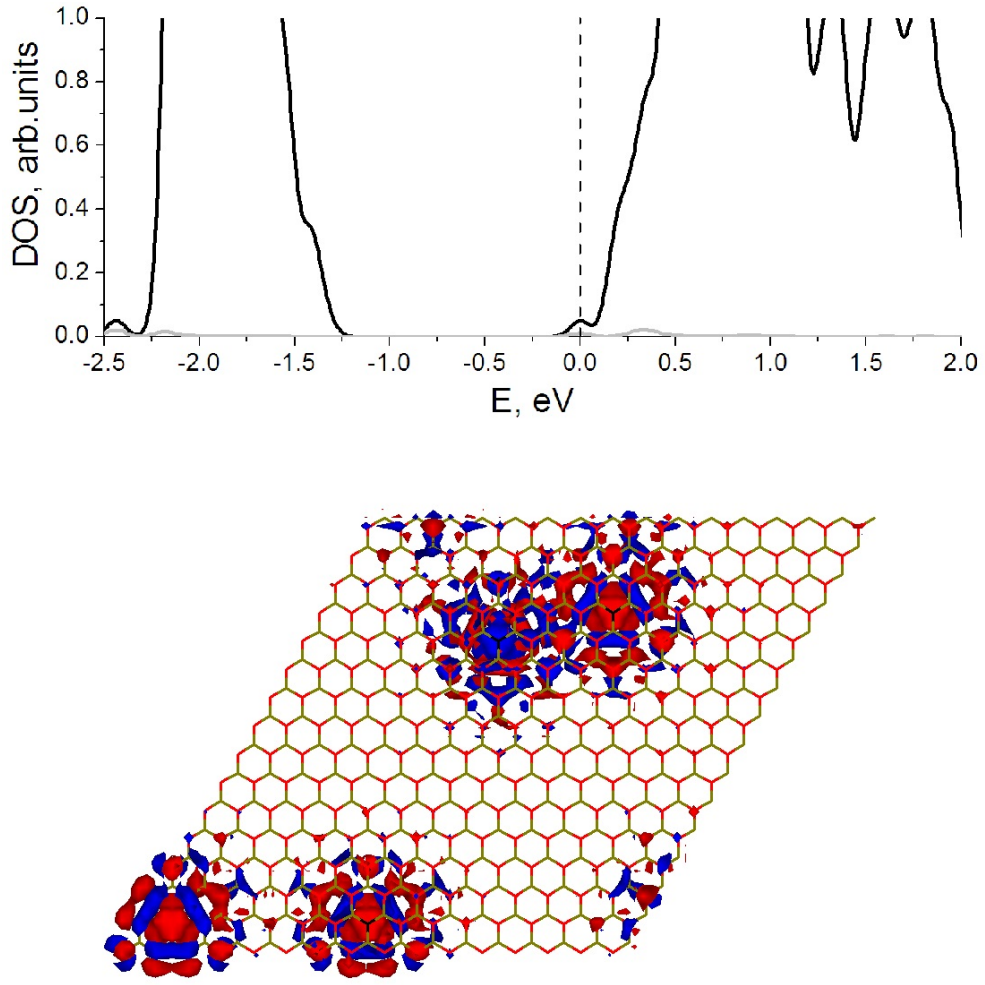

FIG. 8. DOS calculated for the single MoS_2 layer doped by a single Re atom and Γ-point isosurface of the highest occupied crystal orbitals for the single MoS_2 layer with random distribution of Re atoms. Adapted from [59]

atoms having a d occupancy larger than Mo, the ground state is found to be spin polarized, while Y, Zr, and Nb have a diamagnetic ground state. For dopants having occupancy of d-orbitals larger than Re atom, an increasing number of gap states is formed within the band gap, so that the excess electrons do not fill the MoS_2 conduction band. The excess electrons first fill up the majority spin states of the host d-orbitals, until the magnetic moment of the impurity reaches the largest value of 4 μB for Pd. Then, the magnetic moment decreases for Ag and Cd as the additional electrons start to populate the minority spins states. Nb, Zr and Y dopants cause p-type semiconductivity and shift the Fermi level to the top of valence band. The highest states in this band are still delocalized like in pristine MoS_2, therefore, the mobility in MoS_2 upon such p-doping can be expected rather large.

The influence of the doping of non-metal sublattice was also theoretically considered for a semiconducting MoS_2 monolayer. In general, DFT GGA [48] and LSDA calculations [61] give similar results for the change of electronic structure. The doping by atoms of elements with higher number of valence electrons than sulfur (F, Cl, Br, I), leads to n-type character for conductivity with localization of the donor electron near the dopant atom. This situation is quite similar to that for Re doping of Mo-sublattice. The atoms of elements with smaller number of valence electrons (N, P, As and Sb) behave as acceptors. Accordingly, the position of impurity

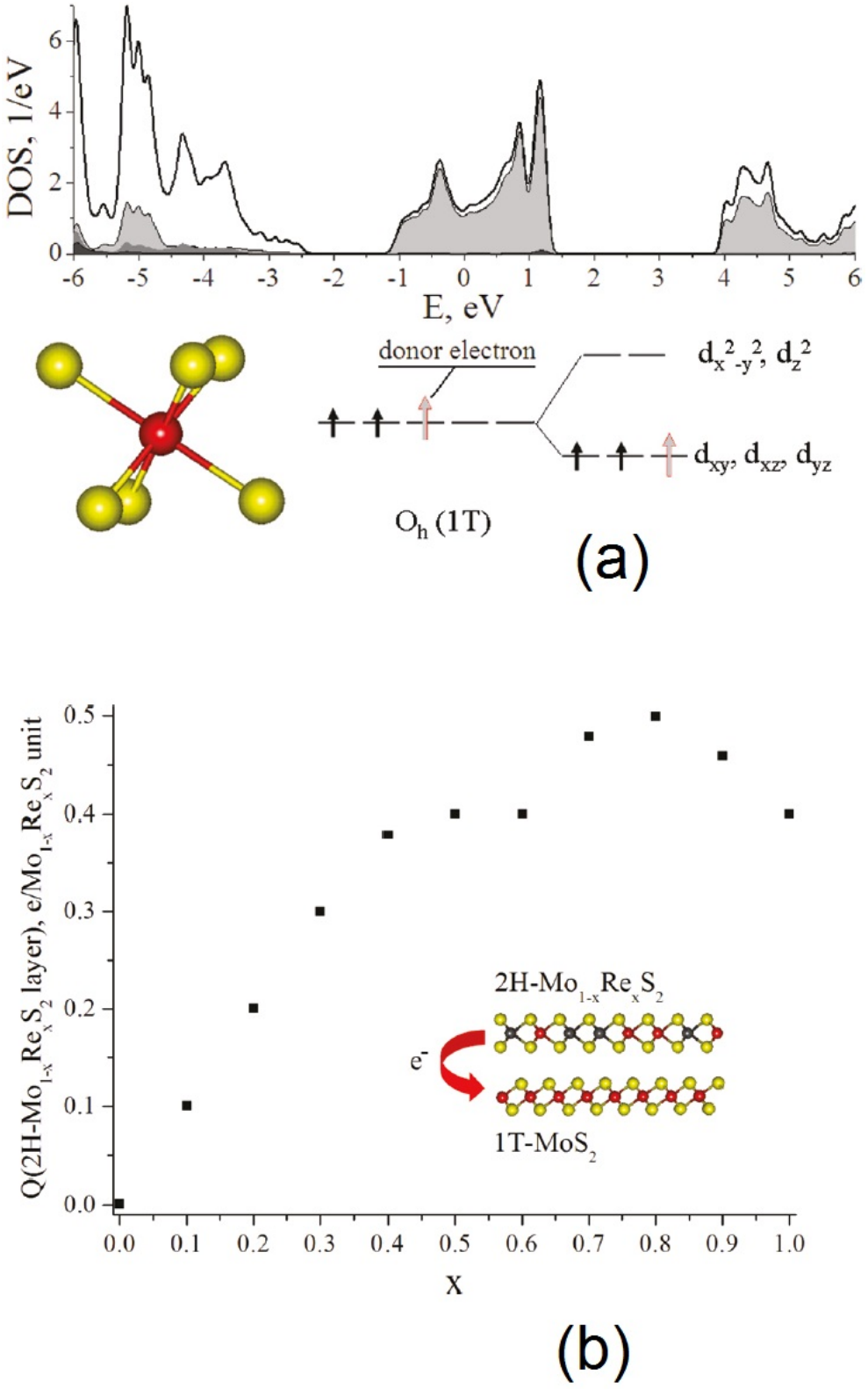

FIG. 9. (a) DOS calculated for the single layer of 1T-MoS_2 phase and ligand field picture for octahedral coordination (Oh symmetry) of Mo atom demonstrating a preferability of electron doping for stabilization of 1T-phase (Mo4d-states are in grey); (b) Charge transfer within double T-MoS_2—H-$Mo_{1-x}Re_xS_2$ layer as a function of the Re content. Adapted from [60]

levels depends on the row number of doping element. Namely, N and P atoms have magnetic moments of about 1 μB and their p-states, hybridized with Mo4d-states, can be found in the band gap of MoS_2 just above the edge of valence band [61]. When the row number is increased, these states shifts towards the valence band, and in the case of As doping, the spin splitting vanishes. The replacement of sulfur by C and Si atoms also leads to p-type conductivity, while the impurity states are well distributed within the valence band of MoS_2.

Isoelectronic doping of MoS_2 monolayer of metal (by M = W) and non-metal (by X = Se or Te) sublattices was investigated by means of DFT GGA calculations [62]. They do not reveal a crucial qualitative change in the band structure. As both pure constituents — MoS_2 and MX_2 — the monolayers of the d-metal chalcogenide solid alloys are semiconductors with direct band gap at the K-point and in the absence of localized states. Thus, the value of the band gap depends on the alloy composition and can be varied between the values of pure compounds, which has potential for the fabrication of a large family of single and a few layer semiconducting chalcogenide materials.

8. Interfaces with the TMCN monolayers

All aforementioned references have been devoted to the properties of the TMCN layers themselves. Though, many variations in the characteristics of a TMCN material can be explained by the measurement conditions and the complexity of a device. While interferences in the 'ideal' electric properties of semiconducting TMCN nanodevices were explained often by the quality of semiconductor itself, the alternative causes can be searched among the environment of semiconductor [62, 63].

Popov et al. suggested that the observed low electron mobility in single layer MoS_2 can be represented not only as an intrinsic material property, but is also biased by unfavorable contacts with the electrodes, i.e. as a MoS_2|metal interface problem [62]. Au is the most common contact metal in the fabrication of electrodes in electronic nanodevices due to the ease of cleaning and high chemical endurance. Yet, this noble inertness, together with the inertness of chemically saturated sulfur within MoS_2 cannot provide an essential bonding during contact and forms a tunnel barrier at the interface, which is not favorable for electron injection into MoS_2. Searching for better contacts than provided by Au, transition metals like Sc, Ti and Zr were suggested as the most suitable candidates with a low work function and good overlapping of their d-orbitals with Mo4d-states. Furthermore, a few basic factors have been taken into account and analyzed comparing with Au using the results of DFT GGA calculations: favorable interface geometry and bonding, the electronic density of states, and the potential barrier at the interface. Among these metals, Ti seems to be an ideal candidate for the modeling due to a small lattice mismatch of Ti(0001) surface with MoS_2 layer.

Comparing with MoS_2|Au(111) surface, the equilibrium separation of contact surfaces within MoS_2|Ti(0001) interface is smaller (2.0 vs 2.6 Å) and calculated binding energy is 2.5 times higher, which indicates good conditions for a larger wave function overlap at MoS_2|Ti interface. This is supported by the DOS analysis (Fig. 10). The most striking difference between MoS_2|Au and MoS_2|Ti interfaces associated with higher DOS at the Fermi level and significant contribution of broadened peaks of S3p and Mo4d_{xy} states in the case of MoS_2|Ti. Electron density maps show a much larger charge carrier density in the interface region between MoS_2 and Ti, than with Au. At the same time, the maps of electrostatic potential and estimated contact tunnel barriers give evidence that electrons in the MoS_2|Ti system have to bypass the much lower and narrower barrier from the metal surface to the delocalized states of MoS_2 layer, than in MoS_2|Au (0.45 eV and 0.9 versus 1.03 eV and 1.59 Å). Thus, Ti could be a more suitable alternative as an electrode material, since it forms a low-resistance Ohmic contact.

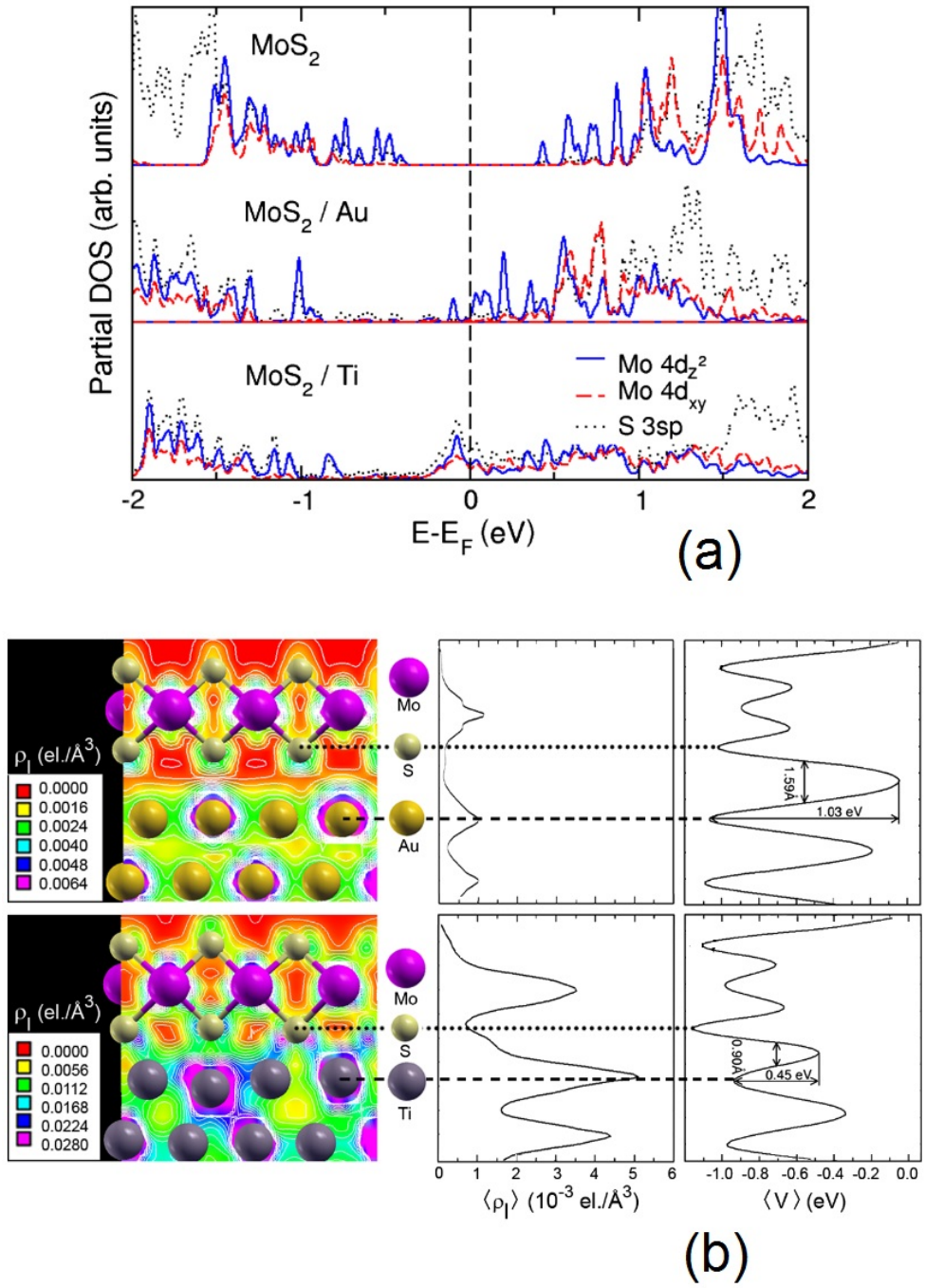

FIG. 10. (a) DOS calculated for the single MoS_2 layer and interfaces MoS_2—Ti(0001) and MoS_2—Au(111); (b) Electronic density $\langle\rho\rangle$ map and electrostatic potential $\langle V\rangle$ along the interfaces MoS_2—Ti(0001) and MoS_2—Au(111). Adapted from [62]

A detailed experimental study of metal contacts to MoS_2 surface was performed for the metals with low work function, such as Sc and Ti as well as with high work function as Ni and Pt [63]. From the temperature-dependent study that considers both thermoionic emissions over the Schottky barrier as well as thermally assisted tunneling, the barrier heights were found as ~ 230, ~ 150, ~ 50 and ~ 30 meV in the row Pt, Ni, Ti and Sc. The field effect mobilities of multilayer micromechanically exfoliated MoS_2 flakes were measured for the case of different metal electrodes and different flake thicknesses using a back-gated geometry. It was found, that the mobility values are strongly determined by the type of metal electrode, i.e. intrinsic mobility is masked by the presence of the aforementioned barrier at the source and drain contacts. Moreover, the mobility of the devices with the top joined source/drain contacts was found to depend on the flake thickness in a nonmonotonic fashion, which suggests an influence of substrate on the performance of FET. While the contacts are directly connected only to the top MoS_2 layer of a flake, the access to deeper layers leads to an additional interlayer resistance. Gating, on the other hand, impacts the deepest layers most, and charge screening results in a decreased number of charges for top MoS_2 layers. For small layer thicknesses, the absence of sufficient screening of the substrate can result in a lower mobility value than observed in the bulk MoS_2. Finally, the highest mobility values were obtained for the flake thickness ~ 10 nm. In this case, the extracted mobility values were found to be 21, 90, 125 and 184 $cm^2/(Vs)$ for Pt, Ni, Ti and Sc contacts, respectively. This is much higher than obtained in earlier studies employing single MoS_2 layer and Au contacts [6–8]. A further significant enhancement in the field effect mobility up to 700 $cm^2/(Vs)$ was achieved by covering the top of the back-gated transistor with high-k dielectric 15-nm-thick Al_2O_3 and in the case of Sc electrodes. This clearly indicated that improving the contact quality and a proper choice of substrate are also essential for obtaining intrinsic material properties.

Dolui et al. have speculated that defects in a high-k dielectric oxide substrate also can affect the conductivity properties of semiconducting TMCN sheets [64]. Charged defects at the surface of such substrate could lead to an inhomogeneous electrostatic potential and serve as charge traps located at the interface. This effect should be most pronounced for a single TMCN layer, where all sheet is in contact with the substrate, and the charged defects at the interface are not screened. In order to affirm a possible role of defects in the substrate on electronic properties of interface, *ab initio* calculations of the DOS were performed for the MoS_2 single layer deposited on a SiO_2 surface with silanol or siloxane termination. As the possible defects of SiO_2 surface the impurity Na or H atoms and O-dangling bonds have been considered. Indeed, a defect-free SiO_2 surface does not affect significantly the electronic properties of these $MoS_2|SiO_2$ interfaces: both the top of valence band and the bottom of conduction band of MoS_2 are located within the wide band gap of SiO_2. However, when a Na or H atom is placed at the interface, a trap state occurs below the conduction band. With Na 'doping', the $MoS_2|SiO_2$ interface becomes a n-type semiconductor with low activation energy, while substituting a H atom forms a trap state located 0.9 eV below the conduction band. In contrast, O-dangling bonds give rise to the states located below the edge of valence band, making $MoS_2|SiO_2$ interface similar to a p-type semiconductor.

9. Concluding remarks

Bulk TMCN layered materials have been explored for a long time due to their highly anisotropic structure. While in the past, the main attention was given to their lubricative and tribological phenomena related with interlayer intercalation, the recent progress in the controlled exfoliation of these compounds allowed the research of their constituents up to the level of single layers. The latter emerges a new perspective of TMCN as the low-dimensional materials for

nanoelectronics applications, especially, for semiconducting TMCNs such as MoS_2 and WS_2. Numerous experimental and theoretical studies of electronic structure of the TMCN sheets have demonstrated a large facility for varying the semiconducting properties, depending on the number of the layers, controlled doping and mechanical action.

Yet, we should accept that the suggested applications still remain in their infancy and cannot yet compete with the Silicon technology, which has been thoroughly evaluated for more than half a century. Despite a long history of TMCN material science and the boosting growth of new results, much of the improvement work should be done already at the level of materials themselves. Former applications of TMCN as the components of antifrictional coatings and lubrication agents did not require high purity materials as is necessary for semiconductor-based electronics. Modern technologies for the fabrication of single and multilayers of TMCNs still do not offer a product, which would be free of native and non-controlled impurities or defects. While latter factors have been theoretically proposed as the drivers for further manipulation of the properties, currently, they should be considered rather as a nuisance. They may essentially restrict proper characterization of the material and limit the performance of devices made from TMCN layers.

Acknowledgments

The support of the ERC project INTIF 226639 is gratefully acknowledged. A. E. thanks grant RFBR 13-03-00272-a.

References

[1] *Physics and Chemistry of Materials with Layered Structures*, **1–8**, Series Eds.: F. Lévy, Springer Netherlands, (1976–1986).
[2] Yang J.F., Parakash B., Hardell J., Fang Q.F. Tribological properties of transition metal di-chalcogenide based lubricant coatings. *Frontiers of Materials Science*, **6** (2), P. 116–127 (2012).
[3] Wilson J.A., Yoffe A.D. The transition metal dichalcogenides discussion and interpretation of the observed optical, electrical and structural properties. *Advances in Physics*, **18** (73), P. 193–335 (1969).
[4] Yoffe A.D. Layer compounds. *Annual Review of Materials Science*, **3** (73), P. 147–170 (1973).
[5] Opalovskii A.A., Fedorov V.E. Molybdenum chalcogenides. *Russian Chemical Reviews*, **35** (3), P. 186–204 (1966).
[6] Novoselov K.S, Jiang D., et al. Two-dimensional atomic crystals. *Proceedings of the National Academy of Sciences of the United States of America*, **102**, P. 10451–10453 (2005).
[7] Radisavljevic B., Radenovic A., et al. Single-layer MoS_2 transistors. *Nature Nanotechnology*, **6**, P. 147–150 (2011).
[8] Ghatak S., Nath Pal A., Ghosh A. Nature of Electronic States in Atomically Thin MoS_2 Field-Effect Transistors. *ACS Nano*, **5** (10), P. 7707–7712 (2011).
[9] Radisavljevic B., Whitwick M.B., Kis A. Integrated Circuits and Logic Operations Based on Single-Layer MoS_2. *ACS Nano*, **5** (12), P. 9934–9938 (2011).
[10] Lagrenaudie J. Comparisondes composes de la famille de MoS_2 (structure et proprietes optiques et electriques). *Journal de Physique et le Radium*, **15**, P. 299 (1954).
[11] Fivaz R., Mooser E. Mobility of Charge Carriers in Semiconducting Layer Structures. *Physical Review*, **163** (3), P. 743–755 (1967).
[12] Späh R., Elrod U., et al. *pn* junctions in tungsten diselenide. *Applied Physics Letters*, **43** (1), P. 79–81 (1983).
[13] Hultgren R. Equivalent Chemical Bonds Formed by s, p, and d Eigenfunctions. *Physical Review*, **40**, P. 891–907 (1932).
[14] Kimball G.E. Directed Valence. *Journal of Chemical Physics*, **8**, P. 188–198 (1940).
[15] Mattheiss L.F. Band Structures of Transition-Metal-Dichalcogenide Layer Compounds. *Physical Review B*, **8** (8), P. 3719–3740 (1973).
[16] Bromley R.A. A semi-empirical tight-binding calculation of the band structure of MoS_2. *Physics Letters A*, **33**, P. 242–243 (1970).

[17] Li T., Galli G. Electronic Properties of MoS_2 Nanoparticles. *The Journal of Physical Chemistry C*, **44**, P. 16192–16196 (2007).
[18] Lebègue S., O. Eriksson O. Electronic structure of two-dimensional crystals from ab initio theory. *Physical Review B*, **79** (11), P. 115409 (2009).
[19] Mak K.F., Lee C., et al. Atomically Thin MoS_2: A New Direct-Gap Semiconductor. *Physical Review Letters*, **105** (13), P. 136805 (2010).
[20] Splendiani A., Sun L., et al. Emerging Photoluminescence in Monolayer MoS_2. *Nano Letters*, **10** (4), P. 1271–1275 (2010).
[21] Komsa H.-P., Krasheninnikov A.V. Effects of confinement and environment on the electronic structure and exciton binding energy of MoS_2 from first principles. *Physical Review B*, **86** (24), P. 241201 (2012).
[22] Kuc A., Zibouche N., Heine T. Influence of quantum confinement on the electronic structure of the transition metal sulfide TS2. *Physical Review B*, **83**, P. 245213 (2011).
[23] Bertolazzi S., Brivio J., Kis A. Stretching and breaking of ultrathin MoS_2. *ACS Nano*, **5**, P. 9703–9709 (2011).
[24] Scalise E., Houssa M., et al. Strain-induced semiconductor to metal transition in the two-dimensional honeycomb structure of MoS_2. *Nano Research*, **5** (1), P. 43–48 (2012).
[25] Li W., Chen J.F., He Q., Wang. T. Electronic and elastic properties of MoS_2. *Physica B*, **405**, P. 2498–2502 (2010).
[26] Li T. Ideal strength and phonon instability in single-layer MoS_2. *Physical Review B*, **85** (23), P. 235407 (2012).
[27] Shi H., Pan H., Zhang Y.-W., Yakobson B.I. Quasiparticle band structures and optical properties of strained monolayer MoS_2 and WS2. *Physical Review B*, **87** (15), P. 155304 (2013).
[28] Ghorbani-Asl M., Borini S., Kuc A., Heine T. Strain-dependent modulation of conductivity in single layer transition-metal dichalcogenides. *Physical Review B*, **87**, P. 235434 (2013).
[29] Seifert G., Terrones H., et al. Structure and electronic properties of MoS_2 nanotubes. *Physical Review Letters*, **85** (1), P. 146–149 (2000).
[30] Teich D., Lorenz D., et al. Structural and electronic Properties of helical TiS2 Nanotubes Studied with Objective Molecular Dynamics. *The Journal of Physical Chemistry C*, **115**, P. 6392–6396 (2011).
[31] Enyashin A.N., Popov I., Seifert G. Stability and electronic properties of rhenium sulfide nanotubes. *Physica status solidi (b)*, **246** (1), P. 114–118 (2009).
[32] Scheffer L., Rosentzveig R., et al. Scanning tunneling microscopy study of WS2 nanotubes. *Physical Chemistry Chemical Physics*, **4**, P. 2095–2098 (2002).
[33] Kaplan-Ashiri I., Cohen S.R., et al. Mechanical behavior of individual WS2 nanotubes. *Journal of Materials Research*, **19** (2), P. 454–459 (2004).
[34] Brivio J., Alexander D.T.L., Kis A. Ripples and Layers in Ultrathin MoS_2 Membranes. *Nano Letters*, **11** (12), P. 5148–5153 (2011).
[35] Lorenz T., Joswig J.-O., Seifert G. Layered Nanostructures — Electronic and Mechanical Properties. *MRS Proceedings*, **1549** (2013).
[36] Podzorov V., Gershenson M.E., et al. High-mobility field-effect transistors based on transition metal dichalcogenides. *Applied Physics Letters*, **84** (17), P. 3301–3303 (2004).
[37] Ayari A., Cobas E., Ogundadegbe O., Fuhrere M.S. Realization and electrical characterization of ultrathin crystals of layered transition-metal dichalcogenides. *Journal of Applied Physics*, **101**, P. 014507 (2007).
[38] Kalikhman V.L., Umanskii Ya.S. Transition-metal chalcogenides with layer structures. *Soviet Physics Uspekhi*, **15** (6), P. 728–741 (1973).
[39] Kaasbjerg K., Thygesen K.S., Jacobsen K.W. Phonon-limited mobility in n-type single-layer MoS_2 from first principles. *Physical Review B*, **85** (11), P. 115317 (2012).
[40] Rouschias G. Recent advances in the chemistry of rhenium. *Chemical Reviews*, **74** (5), P. 531–566 (1974).
[41] Ramakrishna Matte H.S.S., Gomathi A., et al. MoS_2 and WS2 Analogues of Graphene. *Angewandte Chemie International Edition*, **49** (24), P. 4059–4062 (2010).
[42] Coleman J.N., Lotya M., et al. Two-Dimensional Nanosheets Produced by Liquid Exfoliation of Layered Materials. *Science*, **331** (6017), P. 568–571 (2011).
[43] Lauritsen J.V., Kibsgaard J., et al. Size-dependent structure of MoS_2 nanocrystals. *Nature Nanotechnology*, **2** (1), P. 53–58 (2007).
[44] Kim D., Sun D., et al. Toward the Growth of an Aligned Single-Layer MoS_2 Film. *Langmuir*, **27** (18), P. 11650–11653 (2011).
[45] Zhan Y., Liu Z., et al. Large-Area Vapor-Phase Growth Characterization of MoS_2 Atomic Layers on a SiO_2 Substrate. *Small*, **8** (7), P. 966–971 (2012).

[46] Lee Y.H., Zhang X.Q., et al. Synthesis of Large-Area MoS_2 Atomic Layers with Chemical Vapor Deposition. *Advanced Materials*, **24** (17), P. 2320–2325 (2012).
[47] Liu K.K., Zhang W., et al. Growth of Large-Area and Highly Crystalline MoS_2 Thin Layers on Insulating Substrates. *Nano Letters*, **12** (3), P. 1538–1544 (2012).
[48] Komsa H.P., Kotakoski J., et al. Two-Dimensional Transition Metal Dichalcogenides under Electron Irradiation: Defect Production and Doping. *Physical Review Letters*, **109**, P. 035503 (2012).
[49] Komsa H.P., Kurash S., et al. From point to extended defects in two-dimensional MoS_2: Evolution of atomic structure under electron irradiation. *Physical Review B*, **88**, P. 035301 (2013).
[50] Zhou W., Zou X., et al. Intrinsic Structural Defects in Monolayer Molybdenum Disulfide. *Nano Letters*, **13**, P. 2615–2622 (2013).
[51] Van der Zande A., Huang P.Y., et al. Grains and grain boundaries in highly crystalline monolayer molybdenum disulphide. *Nature Materials*, **12**, P. 554–561 (2013).
[52] Enyashin A.N., Bar-Sadan M., Houben L., Seifert G. Line Defects in Molybdenum Disulfide Layers. *The Journal of Physical Chemistry C*, **117**, P. 10842–10848 (2013).
[53] Bollinger M.V., Lauritsen J.V., et al. One-Dimensional Metallic Edge States in MoS_2. *Physical Review Letters*, **87**, P. 196803 (2001).
[54] Erdogan E., Popov I., Enyashin A.N., Seifert G. Transport properties of MoS_2 nanoribbons: edge priority. *European Physical Journal B*, **85** (1), P. 33 (2001).
[55] Najmaei S., Liu Z., et al. Vapour phase growth and grain boundary structure of molybdenum disulphide atomic layers. *Nature Materials*, **12**, P. 754–759 (2013).
[56] Yong K.S., Otalvaro D.M., et al. Calculation of the conductance of a finite atomic line of sulfur vacancies created on a molybdenum disulfide surface. *Physical Review B*, **77**, P. 205429 (2008).
[57] Ghorbani-Asl M., Enyashin A.N., et al. Defect-induced conductivity anisotropy in MoS_2 monolayers. *Physical Review B*, **88**, P. 245440 (2013).
[58] Deepak F.L., Popovitz-Biro R., et al. Fullerene-like $Mo(W)_{1-x}Re_xS_2$ Nanoparticles. *Chemistry — An Asian Journal*, **3**, P. 1568–1574 (2008).
[59] Yadgarov L., Stroppa D.G., et al. Investigation of Rhenium-Doped MoS_2 Nanoparticles with Fullerene-Like Structure. *Zeitschrift für Anorganische und Allgemeine Chemie*, **638** (15), P. 2610–2616 (2012).
[60] Enyashin A.N., Yadgarov L., et al. New Route for Stabilization of 1T-WS2 and MoS_2 Phases. *The Journal of Physical Chemistry C*, **115**, P. 24586–24591 (2011).
[61] Dolui K., Rungger I., Pemmaraju C.D., Sanvito S. Possible doping strategies for MoS_2 monolayers: An ab initio study. *Physical Review B*, **88**, P. 075420 (2013).
[62] Popov I., Seifert G., Tomanek D. Designing Electrical Contacts to MoS_2 Monolayers: A Computational Study. *Physical Review Letters*, **108**, P. 156802 (2012).
[63] Das S., Chen H.-Y., Penumatcha A.V., Appenzeller J. High Performance Multilayer MoS_2 Transistors with Scandium Contacs. *Nano Letters*, **13**, P. 100–105 (2013).
[64] Dolui K., Rungger I., Sanvito S. Origin of the n-type and p-type conductivity of MoS_2 monolayers on a SiO_2 substrate. *Nano Letters*, **13**, P. 100–105 (2013).